

MULTI-BLADE ROW INTERACTIONS IN A LOW PRESSURE RATIO CENTRIFUGAL COMPRESSOR STAGE WITH A VANED DIFFUSER

Kishore Ramakrishnan*
GE Global Research Center
Niskayuna, NY, USA

Simon K. Richards†
GE Global Research Center
Niskayuna, NY, USA

François Moyroud
GE Oil and Gas
Thermodyn SAS
Le Creusot, France

Vittorio Michelassi
GE Oil and Gas
Nuovo Pignone
Florence, Italy

ABSTRACT

Previous experimental and CFD investigation of a GE Oil and Gas centrifugal compressor stage with a vaneless diffuser revealed a complex excitation mechanism caused by an aero-acoustic interaction between three blade rows. In stages with vaned diffusers, additional sources of aeromechanical excitation on the impeller can be expected. This unsteady CFD investigation is a follow-up from the previous vaneless diffuser study to identify any additional sources of excitation that arise in the presence of a vaned diffuser in preparation for aeromechanic tests to be conducted later. The study confirms that excitation from impeller-diffuser interaction generated acoustic modes can dominate the potential field excitation from the diffuser vanes. In addition, a significant aero-acoustic excitation to the impeller at a vane pass frequency corresponding to the sum of the vane counts in the two downstream vane rows is observed, and its origination is discussed. The latter excitation is different from that observed in the vaneless diffuser stage where the vane pass frequency observed by the impeller corresponds to the sum of the vane counts in the upstream and downstream vane rows.

INTRODUCTION

Centrifugal compressor stages have gone through considerable developments since the industrial revolution and the introduction of jet propulsion [1]. They have evolved from

simple and low efficiency designs to high speed, high efficiency and high pressure (ratio) compressors. These developments have been aided by increasingly accurate aerodynamic and mechanical performance predictions and design verification tools, supported by advanced measurement techniques. The current design trend is now towards higher circumferential speeds and pressure ratios, thereby increasing static stresses and dynamic forcing. Consequently, impeller fatigue limit margins are eroding and design experience is being stretched. Hence, the continued development of centrifugal compressors along this trend requires further research and development.

Aeromechanic risk reduction and impeller high cycle fatigue assessment is a multi-disciplinary engineering analysis process. Different levels of analysis must be used depending on the type of stage and machine design and with engineering time constraints. One critical aspect of the analysis process is the identification of the frequency excitations linked to wake/potential field interaction with the impeller and also primary and secondary flow path acoustics. A coincidence in frequency and mode shape between an unsteady excitation and an impeller vibration mode is potentially dangerous. The interference diagram is used to detect aeromechanic crossings early in the design process. For example, Singh et al. [2] presented a blade failure case study and illustrated how the interference diagram can be used to design for high cycle fatigue of the blade leading edge and shroud. For a variable

* Corresponding author. Email: ramakris@ge.com
Mail address: K1-2C37A, One Research Circle, Niskayuna NY 12309, USA.

† Currently affiliated with CD-adapco

speed machine, it is rare to have no crossings over the range of shaft speeds in which the customer wants to operate the compressor. Generally, the crossings must be ranked in order of criticality and an impeller fatigue assessment performed. Impeller forcing amplitudes and aeromechanic damping both contribute to vibratory response and must be quantified. However, although blade forced response analyses may be common in axial machines, they are very much in the early stage of development, validation and application on centrifugal compressors in the Oil and Gas Industry. In fact, a review of the published literature on blade row unsteady aerodynamics and acoustic modes reveals that centrifugal compressors and more generally radial machines have received much less attention than their axial counterparts in these areas, independently of the domain of application.

High-speed high pressure ratio centrifugal compressors for aircraft gas turbine engines are usually equipped with vaned diffusers. The vaned diffuser potential field and/or shock structure is recognized as a significant source of aerodynamic excitation to the rotating impeller. Because of the close spacing between the impeller and the diffuser needed to optimize aerodynamic performance, the non-uniformity of the diffuser potential field can cause a large unsteady force on the impeller blades [3], [4], [5].

The role played by acoustic modes in noise generation in axial turbomachines has received much attention, driven by the stringent noise requirements in the aerospace industry. Tyler and Sofrin [6] presented a theory identifying the nature of spinning acoustic modes generated by rotor-stator interaction in an axial flow compressor. Holste and Neise [7] and Enghardt et al. [8] later extended the theory to multiple rotors and stators. Mengle [9] presented an analysis on the physical aspects of spinning acoustic modes produced by blade vibration, as well as a comprehensive theoretical development to predict and understand the frequency spectra observed in the stationary and rotating frames of reference. Under certain inlet and exit acoustic and aerodynamic conditions, Hanson [10] showed that an acoustic mode could get trapped between blade rows leading to amplification and higher frequency scattering.

While spinning acoustic modes have been studied from a noise generation standpoint, only a small number of experimental and numerical studies have been performed on aeroacoustic sources of high-frequency excitations in low pressure ratio centrifugal compressor stages commonly used in the Oil and Gas Industry. Recently, Konig et al. [11] published an article on shrouded impeller high cycle fatigue and presented two case studies, one based on a 2D impeller stage with a vaned diffuser, the other on a 3D impeller stage with a vaneless diffuser. The authors presented a complex mechanism based on a triple coincidence between an impeller vibration mode, a Tyler-Sofrin excitation resulting from impeller/stator interaction, and secondary flow cavity acoustic modes. In their paper, the authors also discuss CFD results that show that Tyler-Sofrin type acoustic modes can generate stronger forcing on the impeller external diameter than the vaned diffuser potential

field itself. Petry et al. showed test evidence indicating significant interaction between the impeller and the return channel in the presence of a vaned diffuser [12]. However, they mentioned that the CFD could not resolve any such interaction and that further studies were necessary to understand this phenomenon. Also recently, Richards et al. [13] presented a peculiar spinning acoustic mode excitation mechanism in a low pressure ratio compact stage with a vaneless diffuser. The combined experimental and unsteady CFD investigation revealed a complex aero-acoustic interaction between the impeller and the upstream and downstream return channel vanes. This configuration will be later referred to as “CVL”, for Compact stage with VaneLess diffuser.

In this paper, aeroacoustic excitation sources due to blade row interactions in a centrifugal compressor stage with a vaned diffuser are investigated in preparation for upcoming aeromechanical tests. The test rig section and the steady state aerodynamic instrumentation are first introduced followed by the numerical investigation section, where the CFD modeling technique and unsteady simulation results are presented. The discussion summarizes some conclusions specific to low pressure ratio compressor stages, in particular on the amplitude of the acoustic forcing in comparison to the vaned diffuser potential field, as well as the role played by the vaned diffuser in modulating impeller-return channel interactions compared to the CVL configuration.

EXPERIMENTAL INVESTIGATION

Test Rig

The scaled model test rig is presented in Figure 1 below.

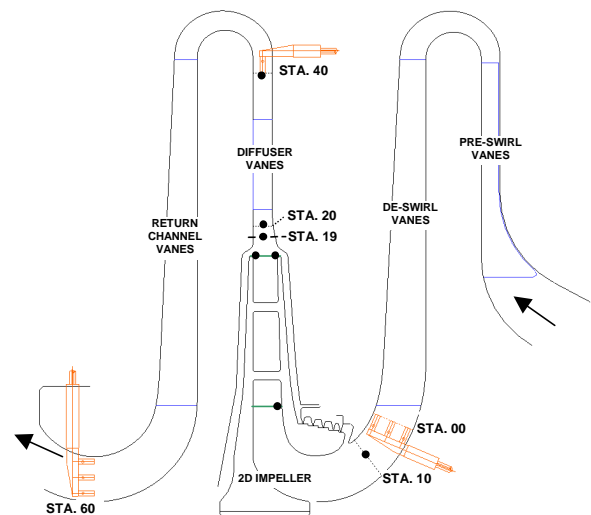


Figure 1: Test rig cross-section and stage configuration, including aerodynamic station numbering and positions of the circumferential arrays of CFD probes (●).

The volumetric flow through the stage is controlled by a downstream valve. The combination of a fixed speed electric

motor and variable speed torque converter allows for variations in shaft speed.

Stage Configuration

The return channel upstream of the impeller has tandem rows of pre-swirl and de-swirl vanes. The first row simulates the presence of an upstream rotating impeller by adding swirl to the flow. The second row is standard for return channels and turns the preswirl exit flow. The flow enters the impeller at an angle dictated by the optimum stage aerodynamic performance. The flow then goes through the impeller and enters the vaned diffuser to initiate pressure recovery. The compressed gas then enters the downstream return channel which has a single row of de-swirl vanes and then exits the test section.

It is necessary to introduce the blade counts for later reference in the results section. Starting with the stators, there are 22 pre-swirl vanes and 22 de-swirl vanes upstream of the impeller, 15 vanes in the diffuser and 22 de-swirl vanes downstream. The impeller consists of 12 repetitive sectors with main blades and splitter blades.

Instrumentation

The stage is equipped with standard steady state aerodynamic instrumentation to measure mass flow, total pressure and temperature at suitable locations and to monitor the operating point and aerodynamic performance of the stage components. Only a subset of that instrumentation is shown in Figure 1. This includes total pressure, temperature and flow angle measurements at stations 00, 20, 40 and 60. At the time of writing, impeller vibration and unsteady pressure measurements are not available for this stage.

COMPUTATIONAL INVESTIGATION

The CFD analysis was performed using a proprietary Reynolds Averaged Navier-Stokes flow solver. The solver is a three-dimensional cell-centered finite volume multiblock, multigrid, structured non-linear and linear unsteady solver for turbomachinery blade row [14] analysis. The solver has a steady and unsteady flow solution capability. For this analysis, a $k-\omega$ turbulence model [15] with the turbulence production term modified as per Launder and Kato [16] is employed. Wall functions are used for near wall treatment. The steady flow solution comprises a central difference spatial discretization scheme incorporating artificial dissipation and multigrid acceleration [17]. Non-linear unsteady solutions are obtained using a dual-time stepping algorithm [18] with multigrid employed to accelerate convergence within each physical time step.

An unsteady CFD analysis was used to determine the impeller loading. For the problem of interest, there is no publically available validation of the unsteady CFD solver. It has however, been validated internally on axial machines, and also shown to correlate with measurements in the CVL stage [13]. The unsteady CFD domain comprises the impeller, the

upstream deswirl, the downstream vaned diffuser, and the return channel vanes. The different blade counts require the full annulus to be simulated to capture all frequencies of interest. The interaction between the blade rows was captured using a sliding mesh boundary condition at the interface between adjacent blade row domains, which allows the transfer of all flow information. To reduce computational effort, the first vane row (i.e., the preswirl) was not explicitly included in the unsteady CFD simulation but its effect accounted for by incorporating the flow distortion generated by this blade row as an input into the inlet boundary condition to the unsteady CFD domain (i.e., the deswirl inlet).

The required modification to the unsteady CFD inlet boundary condition was derived as follows. First, a steady CFD simulation of all five blade rows was performed to determine a steady flow solution representative of the test rig condition. The simulation incorporated one blade passage per blade row with a mixing plane boundary condition used at the interface between neighboring blade rows [19]. Using this solution as a starting point, a second steady CFD calculation was performed which simulated first two vane rows (equal vane counts) only. The sliding mesh boundary condition mentioned previously is employed at the interface between the two vane row computational domains; although in this instance the grid domains are not in motion. Unlike the mixing plane approach, this calculation does not average circumferential non-uniformities and allows the wakes to pass through the blade row interface unaffected. The solution at the deswirl inlet is then extracted to be imposed as an inlet distortion to the non-linear unsteady calculation. Using this approach, excitations to the impeller due to clocking of the first two blade rows are accounted for, without explicitly incorporating the first blade row in the unsteady CFD calculation. Note that the inlet distortion to the deswirl is held to a small perturbation of the time-average boundary condition via a 1-D non-reflecting treatment to account for acoustic waves incident on the boundary from the interior. However, this procedure is only approximate because it does not account for possible acoustic wave reflection from the preswirl.

All blades utilized an O-H type grid topology. A single passage grid for each blade row was generated and then replicated across the full annulus as required. Sufficient grid resolution in each coordinate direction is required to ensure blade wakes are resolved as well as any acoustic waves generated by the interaction of the wakes with downstream blade rows. This resulted in approximately 650,000 elements per blade passage for each blade row simulated and a near wall spacing corresponding to y^+ values below 5 on all surfaces, and below 1 on all impeller surfaces. For the 22 de-swirl vanes, 24 impeller blades, 15 diffuser vanes, and 22 return channel vanes simulated in the unsteady CFD calculation, the total grid element count amounts to more than 55 million. This level of grid refinement with the use of wall functions could possibly introduce some performance modeling inaccuracies; however

an accurate prediction of performance is beyond the scope of the paper.

A temporal resolution of 2880 time steps per impeller wheel revolution was used for the non-linear unsteady CFD calculation. This corresponds to 120 time steps per blade passing period, which adequately resolves the unsteadiness at the frequencies of interest. The calculation ran for five full wheel revolutions in total with approximately 4.8 days of wall clock time for each revolution on a Linux cluster. A periodic unsteady state was reached prior to the completion of the fourth impeller wheel revolution. During the fifth impeller revolution, the solution was sampled to provide data from which the source of the impeller excitation could be determined. To further check for convergence, the solution was run for another two wheel revolutions. Examination of the spectral content of the excitation revealed that the maximum change in harmonic amplitudes for the dominant frequencies of interest is less than 2.5%, from the fifth to seventh wheel revolution, confirming the unsteady convergence of the solution.

Sampling probes are placed in the unsteady CFD domain at several locations. Each probe outputs the flow solution at a single spatial point for each time step of the unsteady calculation. Since there is no aeromechanical instrumentation on the test rig at the time of writing, the CFD probe locations were placed at the blade leading and trailing edges on the impeller, as shown in Figure 1, following the CVL analysis. On the impeller, more probes were placed behind the trailing edge (Station 19) circumferentially at mid-span to help distinguish the acoustic mode content exciting the impeller. Such circumferential probes were also placed at the diffuser inlet (Station 20) and exit (Station 40) as well as the deswirler exit (Station 10) in the stationary frame of reference to provide additional diagnostics on the acoustic excitation.

RESULTS

As mentioned in the introduction, the results of the previous vaneless diffuser centrifugal compressor (CVL) stage analysis will be frequently referenced for comparison to the results presented here. The Tyler-Sofrin theory of spinning acoustic modes was applied to elucidate the excitation mechanism in the CVL stage [13]. According to the theory [6], the circumferential modes generated by the interaction of a rotor and vane row can be determined by $m=nB\pm kV$, where B represents the rotor blade count, V the vane count, n the rotor blade passing frequency (BPF) harmonic, and k is any non-negative integer. In addition to this, when an acoustic wave with a given circumferential mode m interacts with a vane row, it can be partially reflected and scattered spatially into different circumferential modes m' given by $m'=m\pm kV$. The sign convention is chosen such that positive circumferential mode orders spin in the direction of the impeller whereas negative circumferential mode orders spin opposite to the impeller.

Operating Condition

The stage under consideration is a low flow coefficient, low pressure ratio design. Mixing plane, steady state simulations were performed at the design flow coefficient, $\phi = 0.021$, for two different wheel Mach numbers, $\mu=0.3$ and $\mu=0.48$ where the wheel Mach numbers are non-dimensionalized by the inlet stagnation speed of sound. The total pressure variation through the stage is shown in Figure 2 for both wheel Mach numbers. Note that the results henceforth are normalized by the stage inlet total pressure, except when obvious from context.

For both wheel speeds, the computed impeller total pressure ratio compared well with measurements. However, the losses in the diffuser and return channel are slightly under-predicted by the mixing plane multistage analysis. The reason for this could be a combination of turbulence modeling inaccuracies, flow averaging by the mixing plane interface treatment, as well as data averaging in the measurements. The static pressure in the stage also follows a similar trend. Overall, the simulations predict a reasonably good match in impeller and stage pressure ratio.

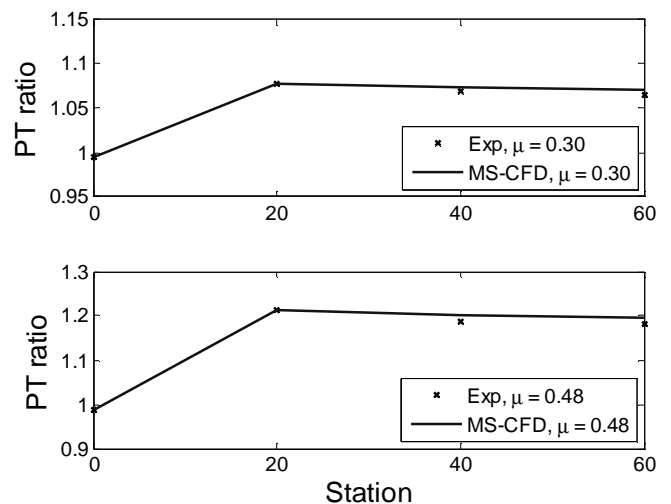


Figure 2: Comparison of predicted vs. measured total pressure rise for design flow coefficient.

While improvements in performance prediction can certainly be investigated, the mixing plane simulation confirms that the CFD operating condition is close to the test condition, providing increased confidence in the nonlinear unsteady analysis. Also, since forcing increases with wheel speed, the higher wheel Mach number (i.e. $\mu=0.48$) operating condition is chosen for the unsteady calculation.

Impeller Leading Edge Unsteady Excitation

The impeller leading edge unsteady excitation is obtained from a Discrete Fourier Transform (DFT) of the probe data from the unsteady CFD analysis sampled over an entire wheel revolution. Figure 3 shows the unsteady pressure frequency

spectrum for the frequencies in the impeller frame of reference (P_n) normalized by the rig inlet total pressure ($P_{T,in}$) at the main or long blade as well as the short blade leading edge.

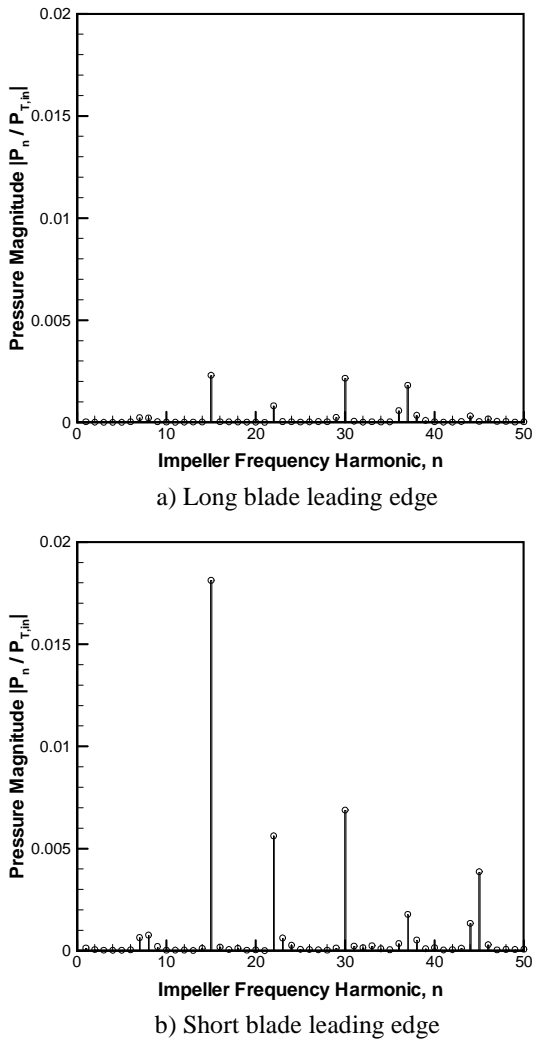


Figure 3: Unsteady pressure spectra from CFD probes on impeller leading edges.

Interestingly, there is hardly any unsteadiness observed at the leading edge of the main blade as evidenced by the spectral content and confirmed by time-domain animation planes (not shown). In contrast to the results for the CVL stage [13], forcing at the 22/rev frequency corresponding to the upstream wakes from the deswirl vanes is very weak. However, at the short blade leading edge, there is comparatively large unsteadiness at multiple frequencies. A possible reason for this could be that the wheel Mach number is higher at the short blade leading edge; hence the higher unsteady 22/rev response. Furthermore, the solidity of the impeller at the short blade leading edge is much higher than at the long blade leading edge, hence cascading

effects could play a role in increased unsteadiness on the short blade suction surface.

Note that there is a strong forcing at the diffuser vane pass frequency (15/rev) and its harmonics at the short blade leading edge. Later it will be shown that these excitations are primarily due to the acoustics generated by impeller-diffuser interaction. Also, the absence of a strong wake excitation indicates that the complex aeroacoustic excitation mechanism observed due to deswirler wake interaction with the impeller in the CVL stage is likely absent in this case.

Impeller Trailing Edge Unsteady Excitation

Figure 4 shows the impeller trailing edge excitation spectra for the long as well as short blades normalized in a manner similar to Figure 3. The spectra shown are near the hub, but are very similar at the shroud.

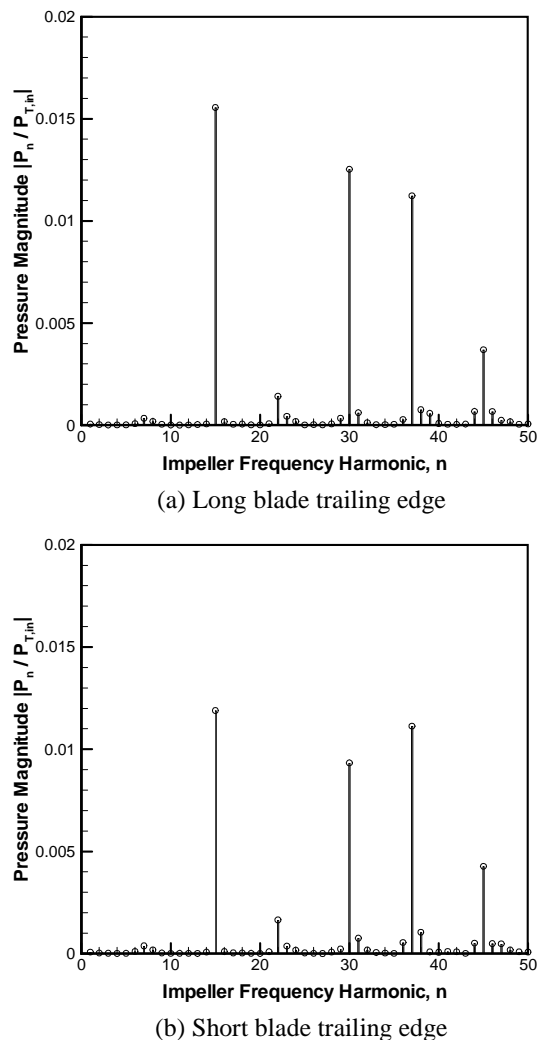


Figure 4: Unsteady pressure spectra from CFD probes on impeller trailing edges.

At the trailing edge, the most dominant excitation is seen at the diffuser vane pass frequencies, namely the 15/rev and its harmonics. There is also a noticeable 37/rev excitation on both blades which corresponds to the sum of either the deswirler (22) and diffuser (15) vane counts, or the return channel (22) and diffuser vane counts. The origination of this excitation will be discussed in detail after interrogating the excitations at the diffuser vane pass harmonics.

Figure 5 shows a correlation map of unsteady pressure from CFD probes placed at Station 19 at mid-span in the impeller frame of reference. The map is generated by a DFT in time of the CFD probe signals over a wheel revolution, followed by a second DFT in space to distinguish forward and backward spinning modes. More details are available in [13]. Note that in Figure 5 and the remainder of the paper, P_{mn} refers to the acoustic mode amplitude with a time harmonic 'n' and circumferential order 'm'.

The temporal frequencies observed in this rotating reference frame are as expected, at the diffuser vane pass frequency and its harmonics (i.e., 15/rev and its harmonics). The 37/rev excitation is also observed. The dominant circumferential modes contributing to these temporal harmonics are indicated by the dashed lines.

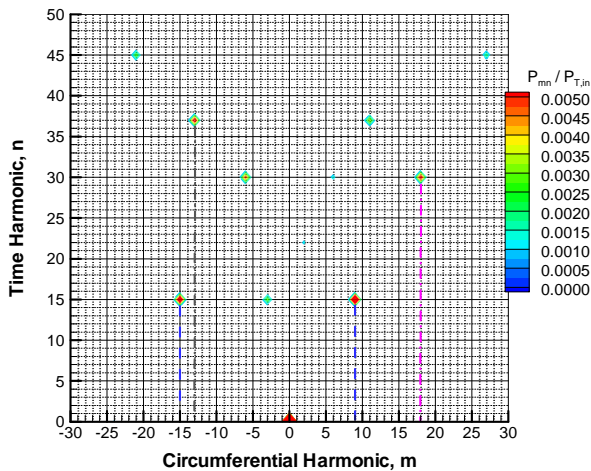


Figure 5: 2D midspan pressure spectra in impeller-diffuser gap at Station 19 (rotating reference frame).

In Figure 5, the 0th time harmonic corresponds to pressure patterns that are circumferentially varying but fixed in time. In this case, the steady, circumferentially averaged pressure field is denoted by the (0,0) mode, and is of no interest to the unsteady problem. Also recall that the sign convention is such that positive circumferential mode orders spin in the direction of the impeller. The $m=-15$ mode at 15/rev is the pressure distortion arising from the first harmonic of the diffuser potential field. The $m=+9$ mode ($+9=24-15$) arises from impeller-diffuser interaction (i.e. 24 impeller wakes interacting with 15 diffuser

vanes) as do the $m=-6$ ($-6=24-2*15$) and $m=+18$ modes ($+18=2*24-2*15$).

In the absence of circumferential mode information in Figure 5, the excitations to the impeller at 15/rev and 30/rev would normally be attributed to the diffuser vane potential field. These are accounted for in the standard design procedure, and present no additional aeromechanical risk. Furthermore, even in those cases where the diffuser generated forcing is high, increasing the impeller-diffuser spacing usually eliminates the problem because the diffuser generated forcing function decays rapidly with increasing spacing. However, in Figure 5, the impeller-diffuser interaction generated acoustic modes are stronger than the diffuser vane potential field. In the impeller frame of reference, the $m=+9$ acoustic mode appears as a 15/rev excitation spinning in the direction of impeller rotation. Similarly, the $m=-6$ and $m=+18$ acoustic modes appear as a 30/rev excitation in the impeller frame of reference.

Figure 6 shows the radial variation at mid-span of the 15/rev forcing in the impeller frame of reference. It is clear that the larger contributor is the acoustic mode generated by the impeller wake-diffuser interaction. This is consistent with what was indicated by Konig et al. [11] and Petry et al. [12].

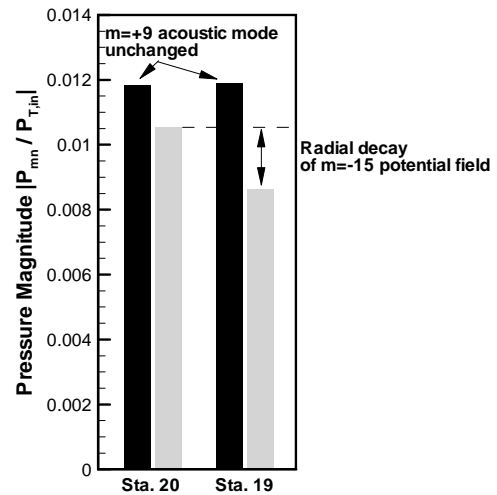


Figure 6: Radial variation of modal contributions to 15/rev.

Figure 6 implies that even if the impeller-diffuser gap were to be increased, the excitation from the acoustic mode would remain even though the potential field forcing would decay radially. In other words, the acoustic modes augment the forcing on the impeller arising from the diffuser potential field. Furthermore, it implies that the unsteady loading on the impeller depends more on the impeller losses and the interaction with the diffuser than the steady loading on the diffuser vanes. This is especially true for the 30/rev as seen in Figure 7 which shows that the acoustic modes dominate the potential field excitation from the diffuser.

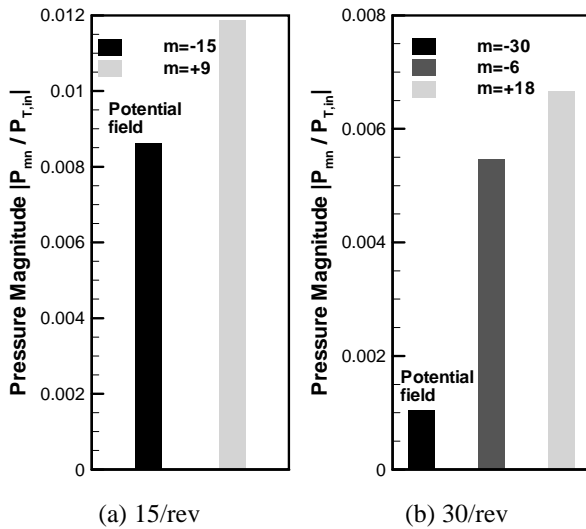


Figure 7: Modal contributions to diffuser vane pass excitations at Station 19.

37/rev Excitation

The impeller trailing edge probe spectra also show a 37/rev excitation that is comparable in magnitude to the 15/rev. From Figure 5, at the 37/rev, two acoustic modes can be seen, the $m=-13$ mode (dominant), and the $m=+11$ mode.

Figure 8 shows the 2D correlation map of unsteady pressure (normalized similar to Figure 5) at mid-span at the vaned diffuser CFD domain inlet (approximately mid impeller-diffuser gap) in the stationary frame of reference. In the stationary frame of reference, the only frequencies observed are at impeller blade passing frequency and harmonics. Thus, the $m=-13$ mode appears at 24/rev and the $m=+11$ mode at 48/rev.

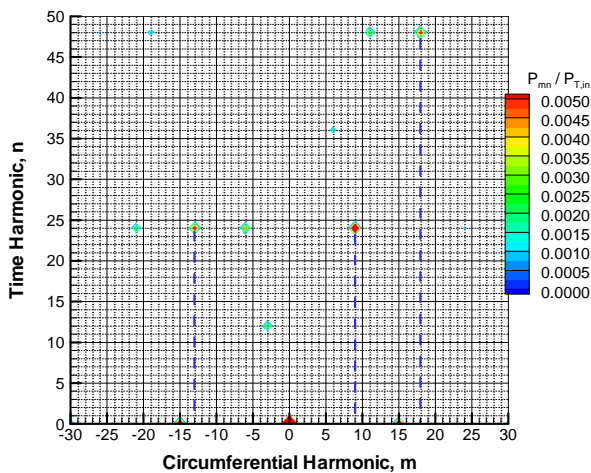


Figure 8: 2D midspan pressure spectra in impeller-diffuser gap at Station 20 (stationary reference frame).

From previous experience with the CVL impeller, it was initially suspected that the 37/rev was caused by an acoustic interaction between the deswirler, impeller and diffuser vanes. In the CVL case, the deswirler wakes interacted with the impeller generating a strong acoustic mode which then propagated downstream, and reflected from the return channel vanes causing an unexpectedly high vibratory response on the impeller. The analogous deswirler-impeller interaction acoustic mode in this case is the $m=+2$ mode ($+2=-22+24$). The reflection of this mode from 15 diffuser vanes could then be responsible for the $m=-13$ ($-13=-2-15$) acoustic mode in Figure 8. The $m=-13$ mode spinning opposite the 24-bladed impeller would then generate a 37/rev excitation on the impeller. However, it is obvious from Figure 8 that the $m=+2$ mode (i.e. the supposed incident mode) is much weaker than the $m=-13$ mode (i.e. the supposed reflected mode). So, the acoustic interaction observed in the CVL impeller does not seem to be at play here, at least not at this operating condition.

A possible explanation for the 37/rev is that it is caused by interaction between the impeller wakes, the diffuser vanes, and the return channel vanes. The mechanism hypothesized is as follows:

1. The impeller wakes interacting with the diffuser generates the $m=+9$ acoustic mode ($+9=24-15$).
2. The $m=+9$ acoustic mode travels downstream and reflects from the 22 return channel vanes as the $m=-13$ mode ($-13=-9-22$).
3. The $m=-13$ mode propagates inward from the return channel, through the diffuser vanes, and is perceived by the 24 bladed impeller as a 37/rev forcing.

The hypothesized impeller-vaned diffuser-return channel interaction mechanism is not far-fetched, as Petry et al. [12][11] mentioned that strong impeller-return channel interaction effects were found in test data.

In order to confirm this mechanism, a 'wave-splitting' analysis similar to that in [13] is performed. The wave-splitting analysis uses a simple characteristic formulation to determine upstream and downstream propagating acoustic modes. Figure 9 shows such a decomposition for the $m=+9$ and $m=-13$ modes at Station 40 in the return channel. The approximate decomposition clearly shows that the $m=-13$ mode is propagating upstream, but unfortunately, the direction is not as clear for the $m=+9$ acoustic mode.

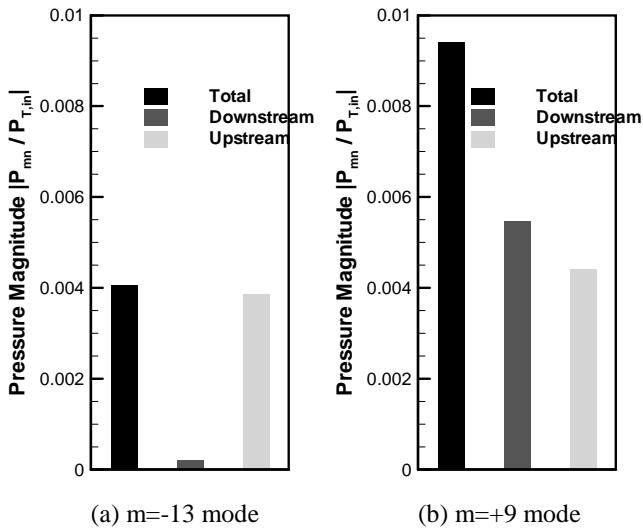


Figure 9: Directional decomposition of dominant acoustic modes in return channel.

While Figure 9 shows that the $m=-13$ mode is upstream propagating, it does not prove that the $m=-13$ mode is caused by the reflection of the $m=+9$ mode. To further support the hypothesized mechanism, an unsteady CFD analysis of the stage is performed at a 40% higher flow coefficient. With increasing flow coefficient, the amplitude of the $m=+9$ mode decreases. Figure 10 shows the mode amplitudes in the return channel at higher flow coefficient normalized by their amplitudes at design flow coefficient.

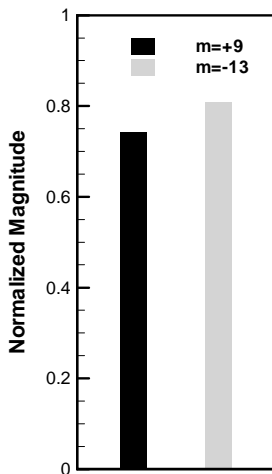


Figure 10: Variation of $m=+9$ and $m=-13$ mode amplitudes in return channel with 40% increase in flow coefficient.

Figure 10 clearly shows that the change in $m=+9$ corroborates the observed change in the $m=-13$ mode at the

higher flow coefficient. Note that the change in amplitude with flow coefficient is not the same for all modes. For instance, the $m=-6$ mode reduces by approximately 80% when the flow coefficient is increased. Thus, the fact that the change in the $m=+9$ and $m=-13$ modes are very similar lends more support to the proposed mechanism

Figure 11 shows the change in 37/rev at the impeller trailing edge with change in flow coefficient. The change in the 37/rev on the impeller in Figure 11 correlates well with the change in the $m=-13$ mode from Figure 10 confirming that the 37/rev is caused by the $m=-13$ mode. This demonstrates that the mechanism of 37/rev excitation is indeed due to the mechanism hypothesized above.

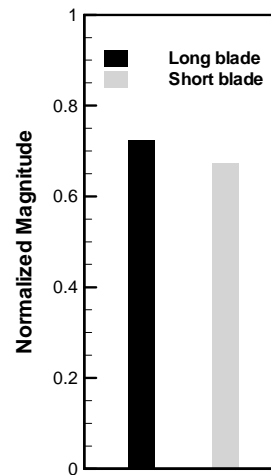


Figure 11: Variation of 37/rev excitation at impeller TE with 40% increase in flow coefficient.

CONCLUSIONS

Previous experimental and CFD investigation of a GE Oil and Gas centrifugal compressor stage with a vaneless diffuser revealed a complex excitation mechanism caused by an aero-acoustic interaction between three blade rows [13]. With the addition of a vaned diffuser to improve performance, additional sources of aeromechanical excitation have been found on the impeller.

The current CFD study shows that excitation from impeller-diffuser interaction generated acoustic modes can dominate the potential field excitation from the diffuser vanes, consistent with recent literature [11], [12]. In addition, a significant aero-acoustic excitation to the impeller at a vane pass frequency corresponding to the sum of the vane counts in the two downstream vane rows is observed (unlike the vaneless diffuser stage [13] where the exciting frequency observed by the impeller corresponds to the sum of the vane counts in the upstream and downstream vane rows).

It must be noted that strong interaction between the impeller and return channel was initially reported in [12] as

being present in test data but not resolvable in CFD and warranting further investigation. The present CFD analysis determines the source and nature of impeller-return channel interaction in the presence of a vaned diffuser for a low-pressure ratio, low flow coefficient centrifugal compressor stage, quantifies the frequency content of this excitation, and confirms that impeller-return channel interactions are a significant source of unsteadiness on the impeller in such stages.

In conclusion, it is important to remember that while CFD provides a valuable diagnostic tool, the acoustic mode generation mechanisms are complex and there may be a large number of these excitations in the operating map of a centrifugal compressor. Furthermore, each Oil and Gas centrifugal compressor design is almost unique because it is tuned to a set of customer specifications and one application. It is difficult to imagine running systematically large-scale unsteady CFD simulations to assess all interference diagram crossings of each compressor. Much more research is needed to arrive at an early detection of an aeromechanic risk in the centrifugal compressor design cycle. This paper is a small step towards this goal.

ACKNOWLEDGMENTS

The authors would like to thank GE Oil and Gas and GE Global Research for funding and for permission to publish this work. We would also like to acknowledge the technical contributions of Silvia Evangelisti, Valeria Ballarini, and Edoardo Cangemi from the Technology Laboratory for the test rig mechanical and instrumentation design, as well as Susanne Svendsdotter and Dante Tommaso Rubino from the Aerodynamics NPI group for the vaned diffuser stage and test design.

REFERENCES

- [1] Krain, H., 2005. "Review of Centrifugal Compressor's Application and Development", *SAE Transactions*, **127**, Issue 1.
- [2] Singh, M.P., Thakur, B.K., Sullivan W.B. and Donald, G., 2003. "Resonance identification for impellers". *Texas A&M 32nd Turbomachinery Symposium Proceedings, Paper T32*, pp. 59-70.
- [3] Dean, R. C., 1974, "The Fluid Dynamic Design of Advanced Centrifugal Compressors", *Lecture Notes Presented at the Von Karman Institute*, Mar 25-29, p 23.
- [4] Sanders, A.J., and Fleeter, S., 1998, "Potential Field Interactions in a Low-Speed Centrifugal Compressor", *AIAA Journal of Propulsion and Power*, Vol. 14, No. 6, pp. 925-933.
- [5] Sanders, A.J., Carnell, W. F., Jr., Oakes, W., Lawless, P. B., and Fleeter, S., 2001, "Characteristics of Potential Forcing Functions in High Speed Centrifugal Compressors", *AIAA Paper 2001-3620*.
- [6] Tyler, J.M. and Sofrin, T.G., 1961. "Axial Flow Compressor Noise Studies". *SAE Transaction*, **70**, pp. 309–332.
- [7] Holste, F. and Neise, W., 1997. "Noise source identification in a propfan model by means of acoustical near field measurements". *Journal of Sound and Vibration*, **203(4)**, pp. 641–665.
- [8] Enghardt, L., Zhang, Y. and Neise, W., 1999. "Experimental verification of a radial mode analysis technique using wall flush mounted sensors". *137th Meeting of the Acoustical Society of America, Berlin, March 15-19*.
- [9] Mengle, V.G., 1990. "Acoustic spectra and detection of vibrating rotor blades, including row-to-row interference". *AIAA Paper 90-3987*.
- [10] Hanson, D.B., 1993. "Mode trapping in coupled 2D cascades - Aerodynamic and acoustic results". *AIAA Paper 93-4417*.
- [11] König, S., Petry, N. and Wagner, N.G., 2009. "Aeroacoustic phenomena in high-pressure centrifugal compressors - A possible root cause for impeller failures". *Texas A&M 37th Turbomachinery Symposium Proceedings, Lecture 9*.
- [12] Petry, N., Benra, K. F., König, S., Woiczinski, C., 2009, "Interaction Between Aerodynamic Phenomena and Impeller Structure of High Pressure Radial Compressors", *8th European Turbomachinery Conference*.
- [13] Richards, S., Ramakrishnan, K., Shieh, C. M., Moyroud, F., Picavet, A., Ballarini, V., and Michelassi, V., "Unsteady Acoustic Forcing on an Impeller due to Coupled Blade Row Interactions", *ASME Paper GT2010-23771*, Proceedings of ASME Turbo Expo 2010: Power for Land, Sea and Air, Glasgow, UK.
- [14] Holmes, D.G., Mitchell, B.E., and Lorence, C.B., 1997. "Three dimensional linearized Navier-Stokes calculation for flutter and forced response". *ISUAAT Symposium*, Sweden.
- [15] Wilcox, D.C., 1993. "Turbulence modeling for CFD". DCW Industries, La Canada, California.
- [16] Launder, B.E., and Kato, M., 1993. "Modeling flow induced oscillations in turbulent flow around a square cylinder", *ASME FED*, **116**, pp. 189–199.
- [17] Jameson, A., 1983. "Solution of the Euler equations for two dimensional transonic flow by a multigrid method". *Applied Mathematics and Computation*, **13**, pp. 327–355.
- [18] Jameson, A., 1991. "Time dependent calculations using multigrid, with applications to unsteady flows past airfoils and wings". *AIAA Paper 91-1596*.
- [19] Holmes, D.G., 2008. "Mixing planes revisited: A steady mixing plane approach designed to combine high levels of conservation and robustness". *ASME Paper GT2008-51296*.